COMMUNICATION

Micrometer-Sized Organic Single Crystals, Anisotropic Transport, and Field-Effect Transistors of a Fused-Ring Thienoacene

By *Rongjin Li, Lang Jiang, Qing Meng, Jianhua Gao, Hongxiang Li,* Qingxin Tang, Meng He, Wenping Hu,* Yunqi Liu,* and *Daoben Zhu*

Charge transport is an essential parameter to estimate the optoelectronic property of organic semiconductors.[1] However, despite years of study, the fundamental aspects of charge transport are still under scrutiny.[2–4] It is imperative to establish the structure–property relationship experimentally to allow the probing of charge transport as a function of molecular arrangement. To approach this scientific target, organic single crystals are good candidates because of their purity, few defects, and long-range order, which are ideal for analyzing the intrinsic properties of organic semiconductors and probing the carrier-transport property as a function of molecular arrangements, for instance, the charge-transport anisotropy.[5] Mobility anisotropy was first demonstrated by Rogers and coworkers in an organic single crystal with the help of the elastomeric transistor stamp technique,[3] which allows relamination of a rubrene single crystal (thin platelets, 0.2 to 1.0 mm thick and 2–3 mm wide) to the source and drain electrodes on an elastomeric poly(dimethylsiloxane) (PDMS) dielectric interface without damaging the crystal surfaces. By rotating the crystal relative to the transistor circuitry (the source–drain–gate electrodes and gate dielectric), mobility variations along different crystallographic directions could be obtained. It was reported that the mobility anisotropy along the *b* and *a* axes (μ_b/μ_a) of the rubrene single crystal was greater than 2.[3] These results were further confirmed by Podzorov and coworkers using an air-gap/free-space technique.[6,7] After that, Kloc and coworkers accomplished such measurements by painting four graphite electrodes on a rubrene crystal,[8] wherein the electrodes could serve alternatively as source or drain electrodes. The mobility anisotropy along the *b* and *a* axes of a rubrene crystal was demonstrated to be greater than 3 in their study, which agreed well with Rogers and Podzorov's results.[3,6,7] Bao[9] and Park[10] designed predeposited radial-shaped electrodes spaced at fixed angular intervals to measure the mobility anisotropy of rubrene or pentacene crystals (typical dimensions of 2–5 mm in width). Their circular array of electrodes incorporated two unique devices at each angular orientation, and offered true 360-degree probing and nearly arbitrary angular resolution. All these pioneering works were well designed and performed, and the methods were applicable for the measurement of mobility anisotropy of other kinds of organic single crystals on specific size scales (such as millimeter size for the crystal handpicking and lamination process).

However, organic crystals always exist as micrometer- or nanometer-sized crystals[11] because of the weak intermolecular interactions of organic compounds, which presents a great challenge for the fabrication of devices, especially for the study of the anisotropic transport property of such ''small'' crystals. The first valuable information about the anisotropy of these ''small'' crystals was demonstrated by Bao and coworkers by drop-casting small crystals on bottom-contact gold-electrode arrays.[12] As addressed by these researchers, a key step in this technique was the selection of crystals with similar, high-quality contacts to the substrate,[12] which influenced the performance of the bottom-contact devices. More recently, Tang, Jiang, and coworkers developed a technique to fabricate transistors with a top-contact configuration based on individual micro-/nanometer-sized ribbons.[13,14] Using this method, the channel length of the transistors could be easily scaled down to the sub-micrometer level, which provided a new and facile method to fabricate devices based on ''small'' organic crystals. Here, this method was further developed and a ''two-dimensional organic ribbon mask'' technique was designed to fabricate organic transistors in situ and non-destructively with a top-contact configuration to probe the transport anisotropy of micrometer- and nanometer-sized organic crystals.

The candidate compound for the anisotropic-transport investigation was dibenzo[*d*,*d*′]thieno[3,2-*b*;4,5-*b*′]dithiophene (DBTDT, Fig. 1a, inset). It is an analogue of pentacene (a benchmark material for organic field-effect transistors[4]) with the same number of delocalized π electrons and the same herringbone crystal structure. Moreover, DBTDT has the advantage of i) easy synthesis on a large scale, ii) high ionization potential, high thermal and photostability, iii) high mobility ($>0.5\ cm^2\ V^{-1}\ s^{-1}$), and high on/off ratio ($>10^6$) of its thin-film transistors.[15] All the advantages suggest that DBTDT would be

[*] Prof. H. Li, Prof. W. Hu, R. Li, L. Jiang, Q. Meng, Dr. J. Gao, Dr. Q. Tang, Prof. Y. Liu, Prof. D. Zhu
Beijing National Laboratory for Molecular Sciences
Key Laboratory of Organic Solids
Institute of Chemistry, Chinese Academy of Sciences
Beijing 100190 (P.R. China)
E-mail: huwp@iccas.ac.cn
Prof. H. Li
Shanghai Institute of Organic Chemistry
Chinese Academy of Sciences
Shanghai, 200032 (P.R. China)
E-mail: lhx@mail.sioc.ac.cn
R. Li, L. Jiang, Q. Meng
Graduate School of Chinese Academy of Sciences
Beijing 100039 (P.R. China)
Dr. M. He
National Center for Nanoscience and Technology
Beijing 100190 (P.R. China)

DOI: 10.1002/adma.200900934

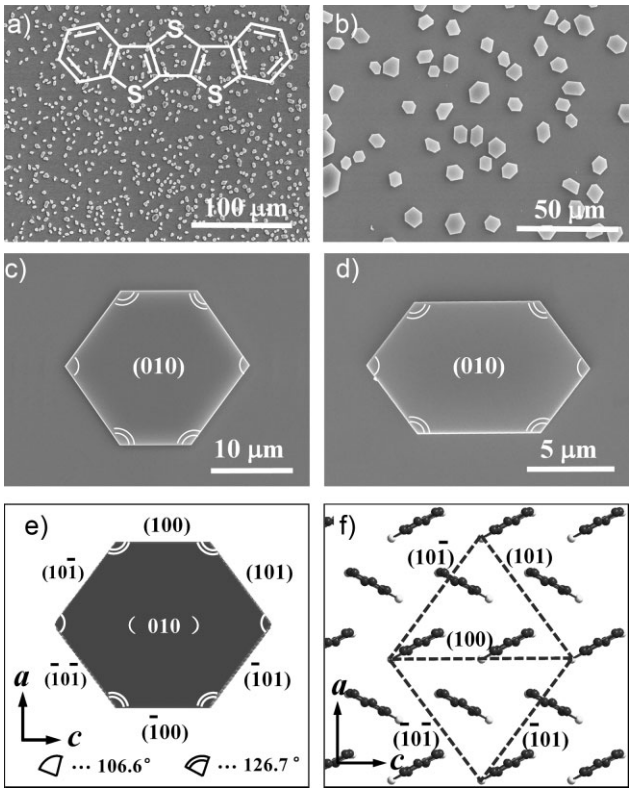

Figure 1. a,b) Large-area SEM images of the hexagonal crystals (the inset shows the chemical structure of DBTDT). c,d) Representative highly regular hexagonal crystals and e) the schematic diagram of the crystal with the facets indexed. f) Herringbone arrangements of the molecules when viewed along the *b* axis (monolayer within the *a*–*c* plane, hydrogen atoms were omitted for clarity). The lines indicate the molecular arrangements along the lateral planes.

extremely valuable for applications in organic electronics. It is therefore attractive for studying the transport properties of its single crystals to approach the intrinsic properties of this material and the transport anisotropy of its crystals to establish the relationship of molecular arrangements and electrical transport.

The synthetic procedure of DBTDT was introduced elsewhere.[15] The single crystals used in this study were grown by the horizontal physical vapor transport (PVT) method.[16,17] DBTDT powder was put in a high-temperature zone, which was stabilized at 140 °C for sublimation, and crystals grew spontaneously on an octadecyltrichlorosilane (OTS)-modified Si/SiO_2 substrate at a low temperature of ~85–100 °C. Typical products are shown in Figure 1a–d. The crystals have regular hexagonal shapes (or elongated hexagonal shapes) with thicknesses ranging from several tens of nanometers to near-micrometer size, depending on the growth period.[18] The single-crystal structure of DBTDT has been determined by Okamoto and coworkers.[19] It belongs to the orthorhombic crystal system, *P*nma space group with $a = 7.933(4)$ Å, $b = 26.589(15)$ Å, and $c = 5.906(3)$ Å. The shapes of the grown crystals were so regular that the crystal facets could be identified directly according to the law of consistency of interfacial angles by inspecting their appearances under an optical microscope (a simple comparison between the measured interfacial angles from the images and the calculated interfacial angles according to the single-crystal structure). An indexed schematic diagram is shown in Figure 1e and the molecular packing (herringbone arrangements) viewing along the *b* axis is shown in Figure 1f. Compared to Figure 1c, the crystal in Figure 1d is elongated along the *c* crystallographic direction. Thus, it is possible that the *c* axis is the fastest crystal-growth direction with the strongest intermolecular interactions.[5] In the case of rubrene and pentacene, the direction of the maximum mobility coincides with the fastest crystal-growth direction.[5] It is, therefore, possible that the maximum mobility of DBTDT is also along the fastest growth direction, namely, the *c* direction.

Devices based on individual micrometer-sized crystals were fabricated following the procedures depicted in Figure 2a–d, which were performed on a Micromanipulator 6150 probe station with a high-resolution microscope (magnification at 400–1000×). First, single crystals of DBTDT were patterned on Si/SiO_2/OTS substrates by PVT from the vapor phase. Then, an individual organic ribbon was picked up and laminated over a patterned crystal. The masks used here were micrometer- or sub-micrometer ribbons of copper phthalocyanine or an anthracene derivative.[13,14] Next, another ribbon was laminated over the previous one at a specific angle (Fig. 2a). After that, Au electrodes (source and drain) were vacuum evaporated on the

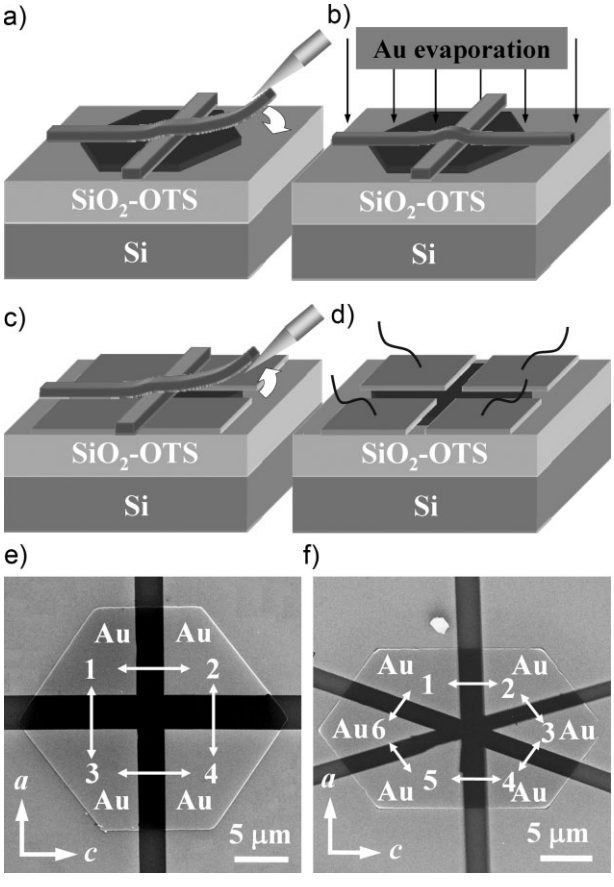

Figure 2. a–d) Processes for the fabrication of electrodes on an individual microcrystal by the ''two-dimensional organic-ribbon mask'' technique. e) SEM image of a transistor with four electrodes to probe the charge transport along the *c* and *a* axes, and f) SEM image of a transistor with six electrodes to examine the transport properties along different crystal planes.

masked structure (Fig. 2b). Finally, the mask ribbons were peeled off by a mechanical probe (Fig. 2c), and the resulting device with four crossed electrodes on an individual hexagonal crystal was obtained (Fig. 2d). A scanning electron microscopy (SEM) image of an exemplified device is shown in Figure 2e. It is obvious that this device configuration (Fig. 2e) was the best for studying i) the field-effect performance of the micrometer-sized single crystals of DBTDT, ii) the anisotropic transport of the crystal along the *c* and *a* directions. It should be mentioned that a third mask ribbon or even more ribbons could be laminated passing through the intersection of the previous mask ribbons or over other parts of the crystal using this method, so that the transport properties along three or more directions of an individual crystal could be measured. For example, six electrodes could be fabricated by this technique on the hexagonal microcrystal (Fig. 2f), which provided a possibility to examine the transport properties of the crystal along different crystal planes, such as the transport along the channels $1 \leftrightarrow 2$, $2 \leftrightarrow 3$, $3 \leftrightarrow 4$, $4 \leftrightarrow 5$, $5 \leftrightarrow 6$, and $6 \leftrightarrow 1$. According to our experience, the mask ribbons should be long and thin enough for the fabrication of high-quality devices. If the mask ribbon is too short, it is difficult to manipulate with a mechanical probe,[13,14,20] and if the mask ribbon is too thick, it cannot contact the substrate intimately by van der Waals forces. In such a case, the ribbons are too easy to move, so that the accuracy of the conduction channels decreases. Because the technique can probe the mobility along different directions within the surface of a crystal, we call our method the ''two-dimensional organic-ribbon mask'' technique.

Representative output and transfer characteristics of the transistors with conduction channels along the *c* and *a* axes are shown in Figure 3. All of the devices exhibited p-type transistor behavior (Fig. 3a). Mobility along the *c* axis was probed to be 0.6–1.8 $cm^2\ V^{-1}s^{-1}$ based on the results of several tens of devices. The highest mobility was ~1.8 $cm^2\ V^{-1}s^{-1}$, as shown in Figure 3b. Moreover, all transistors exhibited very high on/off ratios, which were typically greater than 10^7 (for example, 1.7×10^7, as shown in Fig. 3b). To the best of our knowledge, these are the highest on/off ratios for organic single-crystal transistors. The high on/off ratio of the devices could be assigned to the low-lying highest occupied molecular orbital (HOMO) energy level and wide optical gap of DBTDT.[15] DBTDT had a HOMO level of −5.6 eV,[15] which is lower than that of most p-type organic semiconductors (their HOMO levels are generally between −4.9 and −5.5 eV[21]). Moreover, DBTDT had a wide optical gap of 3.5 eV,[15] which is also much larger than that of most p-type organic semiconductors, for instance, pentacene (1.8 eV[22]). It is obvious that the low-lying HOMO level and wide optical gap are responsible for the high antioxidation stability of DBTDT,[15] as well as the low off current and high on/off ratio of the devices. It should be noticed that the output curves (Fig. 3a) are slightly bent at low V_{DS}, indicating the existence of contact resistance. As is well known, in top-contact transistors the contact resistance is composed of two parts. One is the resistance of the metal/organic interface, which can be determined by the energy-level difference between the Fermi level of the contact metal and the HOMO energy level of the p-type organic semiconductor. The other is the resistance of the organic film/crystal itself between the metal contact and the conduction channel.[23] In this study, the difference between the Fermi level

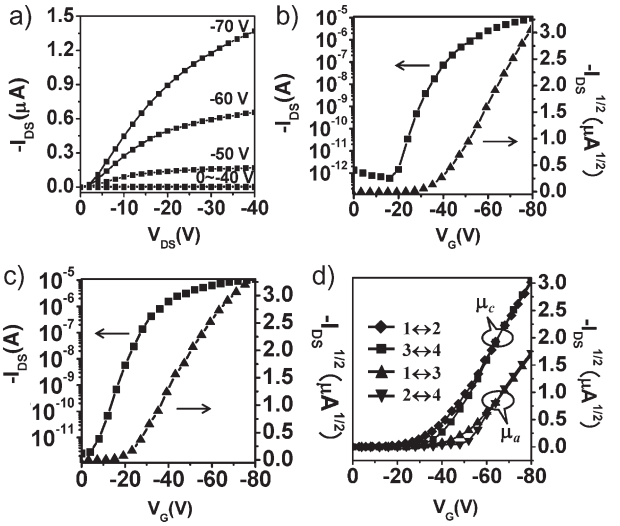

Figure 3. Electrical characteristics of the devices: a) output and b) transfer characteristics (at $V_{DS} = -60$ V, channel width, $W = 5.2$ μm, channel length, $L = 4.8$ μm) of the transistor along the *c* axis. c) Transfer characteristics of the device along the *a* axis (at $V_{DS} = -60$ V, $W = 10.0$ μm, $L = 3.9$ μm). d) The corresponding transfer characteristics of the device shown in Figure 2e, the mobility anisotropy (μ_c/μ_a) of this device was calculated to be 2.3–2.5.

of the Au electrode (5.1–5.2 eV) and the HOMO level of DBTDT (5.6 eV) was mismatched, which might be the reason for the contact resistance.

Compared to the mobility along the *c* axis, the transistors exhibited a much lower mobility along the *a* axis, which ranged from 0.1–0.8 $cm^2\ V^{-1}\ s^{-1}$. Figure 3c shows representative transfer characteristics along the *a* axis. The highest mobility along this direction reached 0.8 $cm^2\ V^{-1}\ s^{-1}$, which was over two times lower than the highest mobility along the *c* axis. Figure 3d shows the transfer characteristics of a device bearing four crossed electrodes (Fig. 2e). The mobility anisotropy (μ_c/μ_a) of this device was calculated to be 2.3–2.5. Tens of measured devices showed the mobility anisotropy (μ_c/μ_a) was around 2–2.5.

It was advantageous that the anisotropy of different crystal planes could also be examined by this method, because the mask ribbons could be laminated over the crystal at any orientation, that is, at any angle with respect to each other according to the crystal shapes. Figure 4a shows an example of such a device schematically and Figure 4b shows the corresponding transfer curves. The conduction channels of $1 \leftrightarrow 2$ and $4 \leftrightarrow 5$ (equivalent directions, μ_c) exhibited the highest mobilities at 0.74 and 0.77 $cm^2\ V^{-1}\ s^{-1}$, respectively. The conduction channels of $2 \leftrightarrow 3$, $5 \leftrightarrow 6$, $3 \leftrightarrow 4$, and $6 \leftrightarrow 1$ (equivalent directions, μ_{ac}) exhibited similar mobilities of 0.47, 0.50, 0.48, and 0.61 $cm^2\ V^{-1}\ s^{-1}$, respectively. The anisotropy μ_c/μ_{ac} of this device was calculated to be 1.2–1.6, which is smaller than that between the *c* and *a* direction ($\mu_c/\mu_a = 2$–2.5).

Although researchers have made great efforts on the predication of field-effect mobility by computer simulation, unfortunately, up to now, an accurate predication is still not possible, and the correlation between molecular packing and field-effect mobility is still not understood thoroughly.[5] It is believed that a closer stacking and stronger intermolecular interactions between adjacent molecules in thin films or crystals

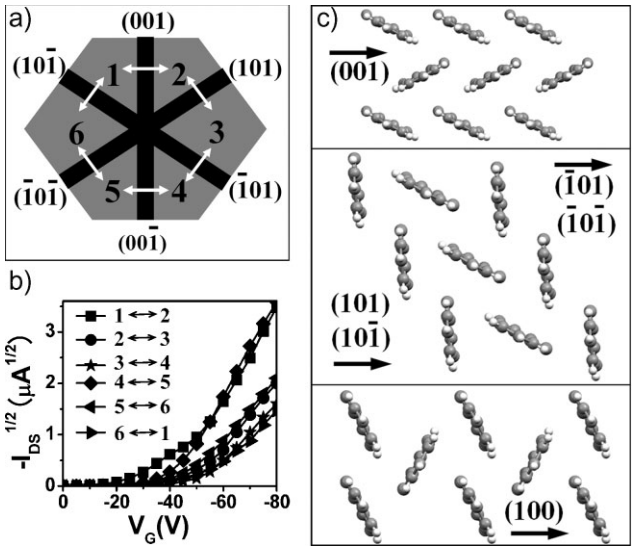

Figure 4. a) Schematic diagram of the transistor with conduction channels parallel to the lateral crystal planes as shown in Figure 2f. b) Transfer curves of different crystal planes. c) The monolayer molecular arrangements along the (001), (101), (10-1), (-101), (-10-1), and (100) planes.

may result in a higher mobility; in other cases a lower mobility is expected.[24–26] For DBTDT, some crystals were elongated along the *c* axis, indicating the *c* axis might be the direction with the strongest intermolecular interactions (Fig. 4c, top). This coincided well with our measurements. The bottom of Figure 4c shows the molecular packing along the *a* axis, which is not as close as that along the *c* axis. The middle of Figure 4c shows the molecular packing of the (101), (10-1), (-101), or (-10-1) planes (within the *a*–*c* plane). The molecular packing is also not as close as that along the *c* axis, but closer than that along the *a* axis. These findings relate well with our experimental results, where the mobility was the highest along the *c* direction and the lowest along the *a* direction. Obviously, the mobility anisotropy is consistent with the fact that the closer the molecular packing, the higher the mobility.

In conclusion, highly regular hexagonal micrometer-sized single crystals of DBTDT were grown controllably by a physical vapor transport technique and transistors based on individual microcrystals were fabricated. The results demonstrated that the transistors exhibited mobilities as high as 1.8 cm^2 V^{-1} s^{-1} with on/off ratios typically $>10^7$. A ''two-dimensional organic-ribbon mask'' technique was developed to fabricate transistors based on an individual microcrystal with multichannels along different crystal axes and crystal planes. The mobility anisotropy along different crystal axes and planes was examined, and it was found that the mobility anisotropy (μ_c/μ_a) was around 2–2.5, which coincided with the fact that the stronger the intermolecular interaction, the higher the mobility.

Experimental

All SiO_2/Si substrates used in this study were successively cleaned by deionized water, ethanol, and acetone. OTS modification was carried out by the vapor-deposition method. SEM images were obtained using a Hitachi S-4300 SE (Japan). *I–V* characteristics of the OFETs were measured using a Keithley 4200-SCS and a Micromanipulator 6150 probe station in a clean and shielded box under air at room temperature. The current resolution of the Keithley 4200-SCS with preamplifier was around 0.1 fA, and the current resolution of the Micromanipulator 6150 probe station was around 30 fA. Hence, the current resolution of the measurement system was around 30 fA.

Acknowledgements

The authors acknowledge the financial support from the National Natural Science Foundation of China (20872146, 50725311, 60736004, 20721061, and TRR61), Ministry of Science and Technology of China, and the Chinese Academy of Sciences.

Received: March 18, 2009
Revised: May 18, 2009
Published online: July 2, 2009

[1] C. D. Dimitrakopoulos, P. R. L. Malenfant, *Adv. Mater.* **2002**, *14*, 99.
[2] H. Moon, R. Zeis, E. J. Borkent, C. Besnard, A. J. Lovinger, T. Siegrist, C. Kloc, Z. Bao, *J. Am. Chem. Soc.* **2004**, *126*, 15322.
[3] V. C. Sundar, J. Zaumseil, V. Podzorov, E. Menard, R. L. Willett, T. Someya, M. E. Gershenson, J. A. Rogers, *Science* **2004**, *303*, 1644.
[4] C. Reese, Z. Bao, *J. Mater. Chem.* **2006**, *16*, 329.
[5] R. W. I. de Boer, M. E. Gershenson, A. F. Morpurgo, V. Podzorov, *Phys. Status Solidi A* **2004**, *201*, 1302.
[6] V. Podzorov, E. Menard, A. Borissov, V. Kiryukhin, J. A. Rogers, M. E. Gershenson, *Phys. Rev. Lett.* **2004**, *93*, 086602.
[7] E. Menard, V. Podzorov, S.-H. Hur, A. Gaur, M. E. Gershenson, J. A. Rogers, *Adv. Mater.* **2004**, *16*, 2097.
[8] R. Zeis, C. Besnard, T. Siegrist, C. Schlockermann, X. Chi, C. Kloc, *Chem. Mater.* **2006**, *18*, 244.
[9] C. Reese, Z. Bao, *Adv. Mater.* **2007**, *19*, 4535.
[10] J. Y. Lee, S. Roth, Y. W. Park, *Appl. Phys. Lett.* **2006**, *88*, 252106.
[11] Q. X. Tang, L. Jiang, Y. H. Tong, H. X. Li, Y. L. Liu, Z. H. Wang, W. P. Hu, Y. Q. Liu, D. B. Zhu, *Adv. Mater.* **2008**, *20*, 2947.
[12] S. C. B. Mannsfeld, J. Locklin, C. Reese, M. E. Roberts, A. J. Lovinger, Z. Bao, *Adv. Funct. Mater.* **2007**, *17*, 1617.
[13] Q. X. Tang, H. X. Li, M. He, W. P. Hu, C. M. Liu, K. Q. Chen, C. Wang, Y. Q. Liu, D. B. Zhu, *Adv. Mater.* **2006**, *18*, 65.
[14] L. Jiang, J. H. Gao, E. J. Wang, H. X. Li, Z. H. Wang, W. P. Hu, L. Jiang, *Adv. Mater.* **2008**, *20*, 2735.
[15] J. H. Gao, R. J. Li, L. Q. Li, Q. Meng, H. Jiang, H. X. Li, W. P. Hu, *Adv. Mater.* **2007**, *19*, 3008.
[16] C. Kloc, P. G. Simpkins, T. Siegrist, R. A. Laudise, *J. Cryst. Growth* **1997**, *182*, 416.
[17] R. A. Laudise, C. Kloc, P. G. Simpkins, T. Siegrist, *J. Cryst. Growth* **1998**, *187*, 449.
[18] R. W. I. de Boer, M. Jochemsen, T. M. Klapwijk, A. F. Morpurgo, J. Niemax, A. K. Tripathi, J. Pflaum, *J. Appl. Phys.* **2004**, *95*, 1196.
[19] T. Okamoto, K. Kudoh, A. Wakamiya, S. Yamaguchi, *Org. Lett.* **2005**, *7*, 5301.
[20] Q. X. Tang, H. X. Li, Y. B. Song, W. Xu, W. P. Hu, L. Jiang, Y. Q. Liu, X. K. Wang, D. B. Zhu, *Adv. Mater.* **2006**, *18*, 3010.
[21] R. Murphy, J. M. J. Fréchet, *Chem. Rev.* **2007**, *107*, 1066.
[22] T. Yasuda, T. Goto, K. Fujita, T. Tsutsui, *Appl. Phys. Lett.* **2004**, *85*, 2098.
[23] T. Minari, T. Miyadera, K. Tsukagoshi, Y. Aoyagi, H. Ito, *Appl. Phys. Lett.* **2007**, *91*, 053508.
[24] J. L. Brédas, J. P. Calbert, D. A. da Silva Filho, J. Cornil, *PNAS* **2002**, *99*, 5804.
[25] J. L. Brédas, D. Beljonne, V. Coropceanu, J. Cornil, *Chem. Rev.* **2004**, *104*, 4971.
[26] L. Q. Li, Q. X. Tang, H. X. Li, X. D. Yang, W. P. Hu, Y. B. Song, Z. G. Shuai, W. Xu, Y. Q. Liu, D. B. Zhu, *Adv. Mater.* **2007**, *19*, 2613.